Fast and accurate extraction of complex permittivity from surface imaging with SPDR scanner and hand-held VNAs

Olga Stec
Military University of Technology
QWED. Sp. z o.o
Warsaw, Poland
ostec@qwed.eu

Marzena Olszewska-Placha
QWED. Sp. z o.o
Warsaw, Poland
molszewska@qwed.eu

Janusz Rudnicki
QWED. Sp. z o.o
Warsaw, Poland
jrudnicki@qwed.eu

Malgorzata Celuch
QWED. Sp. z o.o
Warsaw, Poland
mceluch@qwed.eu

***Abstract*— The work proposes and validates a methodology for efficient imaging of material samples with a recently developed portable 2D scanner incorporating a 10 GHz split-post dielectric resonator and driven by a low-form-factor vector or scalar network analyser. First, experimental studies are conducted to evaluate the influence of the network analyser operating parameters on the accuracy and stability of complex permittivity extraction. The settings of 1 kHz intermediate frequency bandwidth and 200 frequency points within the measured band are selected, as a cost-to-accuracy compromise. Then, a post-processing procedure based on Lorentzian curve fitting is applied to the raw response, to further enhance the measurement accuracy and stability. The methodology is applied to three materials, and a 2D scan of a laminate sample demonstrates the achieved efficiency.**

Keywords—material measurements, non-destructive testing, 2D imaging, dielectric resonators, split-post dielectric resonator, SPDR scanner, network analysers, curve fitting, Lorentz curve

I. Motivation and Outline of the Work

Dielectric resonator (DR) measurement techniques have been extensively discussed in the literature [1-3] and have a well-established position of precise measurement methods ensuring high accuracy of material parameters extraction [5]. This primarily concerns a split-post dielectric resonator (SPDR) [1], which is recognised for its supreme accuracy [5,6] and will be subject of the present paper, but also a single-post dielectric resonator (SiPDR) [2], a balanced-type circular disk resonator (BCDR) [3], and a Fabry-Perot Open Resonator (FPOR) [4], to name the most popular ones, covering different materials in different frequency ranges.

Recently, extensive research efforts are put to developing novel materials, such as polymer composites, carbon- [7,8] or silver-based [9] or organic semiconductors [10], found to have appealing electrical or electro-chemical properties, promising in application to printed electronics [11] or in energy storage systems [10]. The manufacturing process, which often includes mixture milling to break agglomerates of conductive inclusions and different deposition techniques, such as screen printing [12] or spin-coating [13], may to a great extent influence lateral homogeneity of electromagnetic parameters of the material. Therefore, 2D imaging test fixtures such as the recently reported 10 GHz SPDR scanner [14,15], gain a continuously growing importance in material characterisation techniques.

In DR measurements, accuracy of the retrieved material parameters depends on the accuracy of measuring the resonant frequency and Q-factor for the resonator, with and without the sample under test (SUT). This in turn depends on the performance and settings of the microwave active devices used for signal generation and Q-factor extraction, i.e., Vector Network Analysers (VNA) of different form-factors or scalar analysers such as Q-Meters [15, 16]. While professional VNAs are equipped with many options enhancing the measurement accuracy, they are destined for laboratory use and typically remain beyond the reach of non-microwave engineers such as chemists or biomedical scientists dealing with novel materials. On the other hand, even lower-cost easy-to-use hand-held analysers offer two parameters decisive in our considerations, namely, the number of frequency points at which the measurement is conducted (NbFP) and the width of the applied intermediate frequency bandwidth (IFBW). Increase of NbFP and decrease of IFBW lead to higher accuracy of the resonant frequency and Q-factor extraction, however, at the cost of longer measurement times. For a single DR measurement, as regulated by the IEC norm [5] and typically reported in the open literature [1-4], time is not a critical issue. It is then admissible to use low IFBW, leading to high signal-to-noise ratio and accurate measurement of material parameters, averaged within the DR "head" (SUT area interacting with the DR). However, in DR applications to 2D imaging, where the measurement is conducted over a grid of hundreds or thousands of points over the SUT, such an approach becomes ineffective and even prohibitively time-consuming, as we further demonstrate.

This work concerns the recently reported 10 GHz SPDR-based 2D scanner [14,15], developed within the EU H2020 MMAMA project [17]. The scanner is compatible with different form-factor microwave devices and has been operated with a dedicated Q-Meter [15] as well as a general-purpose hand-held VNA FieldFox N9918A [14]. For

reference, herein we also connect the scanner in its test (static) mode to a fully-fledged bench-top Keysight N5245A PNA-X, further called LabVNA. Our goal is to propose a material characterisation methodology producing accurate and stable 2D maps of complex permittivity within acceptable measurement times. This is accomplished in two steps:

- Through a series of experiments utilising both FieldFox and LabVNA, and three SUTs of different materials, we study the accuracy and stability of SPDR measurements. We heuristically select such settings of IFBW and NbFP, which appeal as a good starting point for further post-processing.
- We implement a post-processing procedure based on fitting the raw measured data to the theoretical Lorentzian resonance curve.

We finally demonstrate that the proposed approach enhances the accuracy and stability of SPDR measurements and allows efficiently imaging our target samples.

II. Stability and Accuracy of SPDR Measurements

Fig. 1 shows a photo of the portable scanning setup after [14,15] connected to FieldFox. The Master Unit Control Application (MUCA) mechanically controls the scanner and invokes microwave measurements. Two example curves of power transmission through the empty resonator are presented in Fig. 2. With the increased intermediate frequency bandwidth, the noise content increases. Using raw measurements, the user extracts the resonant frequency as the frequency f_0 where the |S21| curve has a maximum, and Q-factor from the 3dB bandwidth, calculated between the two points closest to f_0 from left (f_{min}) and right (f_{max}), where |S21| drops by 3dB. It is deduced from Fig. 2 (and confirmed by our numerous experiments) that in the presence of the noise, the shift of the extracted f_0 caused by the noise may be up or down in frequency (even though the maximum value of noisy |S21| will always be overestimated); the frequencies f_{min} and f_{max} will always be too close to f_0, resulting in the underestimated 3dB bandwidth and overestimated Q-factor.

Professional VNAs often come with firmware, which accurately extracts the resonant frequency and 3dB bandwidth from noisy curves, often based on both amplitude and phase of S21. Similarly, professional microwave engineers are able to perform a kind of "smoothing" and "averaging" by just carefully observing the displayed curves. In our MMAMA project work on portable devices for use in a broad range of material industries [17], we need to rely on raw |S21| measurements. Moreover, the resonant frequencies and Q-factors need to be automatically extracted, converted to the material data, and presented to a non-microwave specialist. As such, we can afford to make a (single) reference measurement of the empty SPDR with low IFBW; however, during the scanning, as fast operation (and hence as high IFBW) as reasonably accurate are needed.

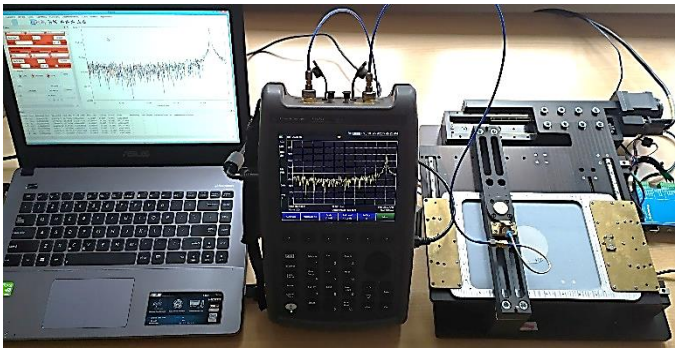

Fig. 1. A photo of the imaging system built of (from right to left) the 2D SPDR scanner with a quartz sample, FieldFox, and a laptop running MUCA.

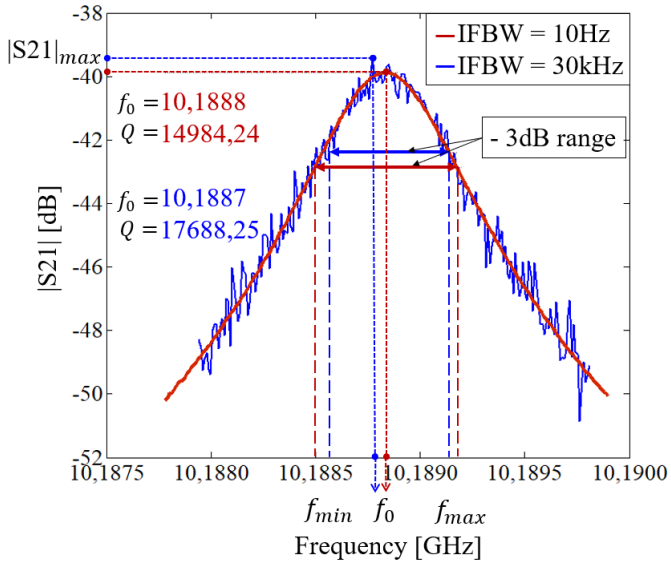

Fig. 2. Example power transmission through the empty SPDR measured at 200 frequency points, with two different IFBW settings of Field Fox, corresponding to SNR of ca. 50 dB (IFBW=10Hz) and SNR of ca. 30 dB (IFBW=30kHz).

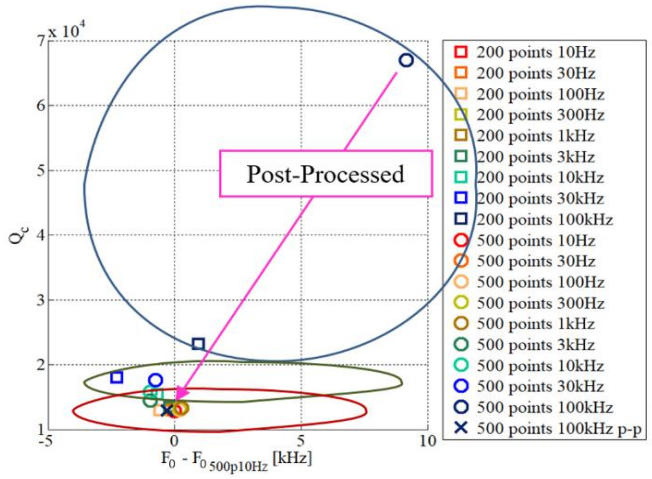

Fig. 3. Example raw measurements of quartz, in the system of Fig. 1, for different settings of IFBW (colours) and NbFP (squares ocircles); the cross marks the result of the proposed post-processing of the least-accurate raw measurement.

Fig. 3 presents an example set of FieldFox measurements of a quartz sample. Herein and further in this work, the empty SPDR is characterised with the lowest available IFBW=10Hz and the highest available number of 500 frequency points per

frequency band. Here, also one measurement of the SPDR loaded with quartz is performed with the above settings, for reference, and then a series of measurements (F_c, Q_c) have been made with IFBW varying between 10 Hz (red marks in Fig. 3) and 100 kHz (navy blue), and either 200 (squares) or 500 (circles) frequency points. The results of Fig. 3 confirm that high IFBW (navy blue) imposes the noise, which leads to de-tuned resonance and overestimated Q-factor. We actually see that the results can be grouped into three "clouds" depending on IFBW, from accurate red through intermediate green up to inaccurate blue. The value of NbFP is less relevant.

We finally postulate that the choice of NbFP=200 and IFBW=1 kHz (brown square) produces the result in close proximity of the most accurate measurement, in a reasonably short time (ca. 156 times shorter than needed with the highest precision of NbFP=500 and IFBW=10 Hz). Validation of this claim will be presented in Section IV.

III. Measurements Fitting to Lorentzian Curve

The methodology proposed in this work assumes performing fast and potentially rough measurements of |S21| (but with the above selected values of IFBW and NbFP, being a compromise between accuracy and time) and afterwards applying a post-processing algorithm to smooth the curve of |S21| and enhance the accuracy of the extracted material parameters. Several curve-fitting algorithms to different analytical curves have been tested, using e.g. polynomials of different order, and the best results have been obtained by fitting to a Lorentzian resonance curve:

$$z(f) = \frac{z_0}{\sqrt{1 + Q^2\left(\frac{f}{f_0} - \frac{f_0}{f}\right)}} \qquad (1)$$

where z_0 stands for amplitude in resonance, Q is a quality factor, f_0 is resonant frequency.

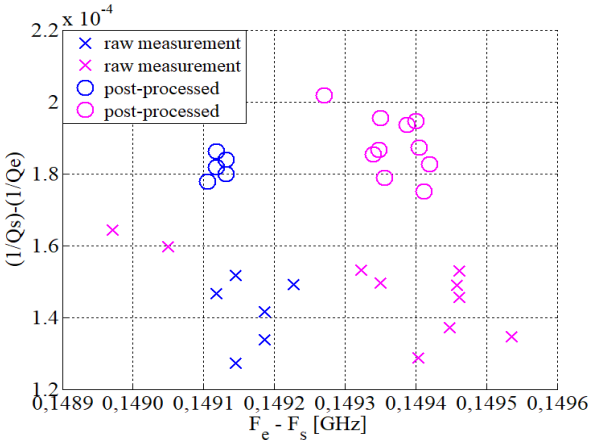

Fig. 4. Resonant frequency de-tuning and Q-factor decrease caused by a laminate SUT, measured in the system of Fig. 1 with FieldFox (IFBW=1kHz, NbFP=200): two extreme series of measurements, raw and post-processed.

Notably, the function in (1) represents impedance variation versus frequency for a simple RLC resonant circuit. In the case of dielectric resonators for material measurements, which are high-Q and typically weakly coupled to the microwave system (see |S21| below-40dB in Fig. 2), this function is also a good approximation of the transmission, which explains its relevance to our post-processing approach. With reference to Fig. 2, we now apply the post-processing to the most extremely diverged result for the raw measurement of quartz (navy blue circle, IFBW=100 kHz) and we see that it is transformed into a navy blue cross, in the proximity of the most accurate (lowest IFBW) raw measurements.

IV. Experimental Validation

We further consider a piece of a laminate as a sample-under-test. We perform many series of measurements in the system of Fig. 1, in the same room but on several different days, hence in somewhat different ambient conditions. Before each series, we measure the empty SPDR (producing F_e and Q_e in Fig. 4) and then measure the SPDR loaded with SUT several times (producing F_s and Q_s in Fig. 4). In Fig. 4, blue and magenta crosses mark the results of the two apparently most diverged measurement series. Our post-processing procedure (respective circles) correctly reveals higher losses (lower Q_s) than those obtained from the raw data. Also, each of the "clouds" of circles is more focused than its corresponding "cloud" of crosses, which implies a better short-term stability of complex permittivity measurements. The proposed post-processing algorithm can therefore be considered as contraction mapping, though a corresponding mathematical proof is beyond the scope of this work.

The distance between the two "clouds" of circles in Fig. 4 represents the long-term stability of our measurement methodology and should be within the accuracy requirements dictated by the standards [5,6] which average to 0.3% for flat homogeneus SUTs of uniform thickness.

We verify our compliance with the SPDR accuracy standards for three samples: the already considered quartz and laminate, and a piece of foam. Table I shows their permittivities and loss tangent obtained with a professional LabVNA (Keysight N5245A PNA-X), with its most accurate settings (and longest measurement times).

In the system of Fig. 1, we perform several series of fast measurements of all SUTs with FieldFox. Within each series, we extract dielectric constants and loss tangents, and calculate their average values as well as spread (within each series). For each SUT, the results collated in Tables II and III correspond to the two series, which produce the lowest and highest values of its average dielectric constant. For quartz and foam, the relative discrepancy (long term stability) is within 0.2%, i.e., within the rule-of-thumb 0.3% standard. For laminate, the discrepancies reach 0.98%, which is attributed to the SUT's thickness nonuniformity, which adds to the measurement accuracy margin as explained in [1,5,6].

TABLE I. Reference Dielectric Constant and Loss Tangent Extracted with LabVNA Measurements

SUT	REFERENCE FROM LabVNA (NbFP 1000, IFBW 10Hz)	
	ε'	tanδ
Foam	1,1281	0,0031
Quartz	3,8248	0,0002
Laminate	3,6857	0,0049

TABLE II. SHORT-TERM STABILITY OF MATERIAL PARAMETERS EXTRACTED FROM RAW AND POST-PROCESSED FIELDFOX MEASUREMENTS: SERIES 1 "BLUE"

SUT	Field Fox (NbFP 200, IFBW 1kHz) short term			
	raw		post-processed	
	ε'	tanδ	ε'	tanδ
Foam	1,1280 ±0,0013	0,0027±0,0002	1,1281±0,0004	0,0027±0,0002
Quartz	3,8253 ±0,0007	0,00011±0,00006	3,8254±0,0004	0,00017±0,00002
Laminate	3,6790±0,0050	0,0036±0,0004	3,6806±0,0013	0,0046 ±0,0003

TABLE III. SHORT-TERM STABILITY OF MATERIAL PARAMETERS EXTRACTED FROM RAW AND POST-PROCESSED FIELDFOX MEASUREMENTS: SERIES 2

SUT	Field Fox (NbFP 200, IFBW 1kHz) short term			
	raw		post-processed	
	ε'	tanδ	ε'	tanδ
Foam	1,1296±0,0008	0,0029±0,0003	1,1295±0,0004	0,0033±0,0001
Quartz	3,8240±0,0008	0,00012±0,00004	3,8243±0,0005	0,00017±0,00003
Laminate	3,6775±0,0010	0,0034±0,0003	3,6766 ±0,0002	0,0045 ±0,0001

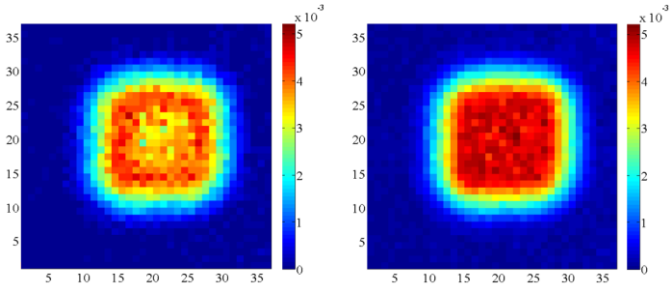

Fig. 5. Loss tangent map of a 15 mm x 15 mm laminate SUT, obtained from raw (left) and post-processed (right) FieldFox measurement with IFBW=1 kHz and NbFP=200. The right image would not not visibly differ from the high-precision scan (IFBW=10 Hz, NbFP=500).

Having demonstrated the accuracy of the proposed approach, we now show its efficiency in surface imaging. We scan a 15 mm x 15 mm sample of a laminate, placed on a microwave-transparent background of 31 mm x 31 mm, with a spatial resolution of 1 mm, resulting in 961 measurement grid points. Admittedly, the 8 mm margins around the SUT are scanned to accommodate the head of our 10 GHz SPDR (ca. 16 mm in diameter). This provides the necessary information for further planned resolution enhancement with the Space Domain Implicit Technique (SDI) after [18].

The total imaging time of 961 grid points with the system of Fig. 1, with the previously selected FieldFox settings (IFBW=1 kHz, NbFP=200), and including the post-processing of Section III and material parameter extraction, is around 1 h 33 min. The images of the loss tangent obtained from the raw (left) and post-processed (right) data are shown in Fig. 5. Clearly, the latter image is more uniform within the SUT, while the first one is corrupted by the measurement noise. - The edges are diluted in both cases, due to the finite SPDR head, and edge resolution enhancement by SDI will be subject of future work.

Now, consider the SUT interior of 10 mm x 10 mm. The average values and spread of the loss tangent images produced from the raw and post-processed data, respectively, are 0.0035±0.0013 and 0.0047±0.0005. The latter values are within the previously (Tables II and III) observed spread from the reference LabVNA measurement (Table I). To the contrary, losses extracted from the raw data are underestimated and corrupted by 2.5x bigger spread over the SUT interior.

For comparison, the same scan performed with the most accurate FieldFox settings (IFBW=10 Hz, NbFP=500) would require ca. 3 days, producing permittivity images of the same quality (in terms of average and spread) as that of Fig. 5, right. This is not only 50 times slower than the proposed approach, but hardly acceptable for industrial materials characterisation.

V. CONCLUSIONS

We have proposed a methodology for fast and accurate imaging of material surfaces with the SPDR scanner and low form-factor network analyser. When FieldFox is applied in this role, the settings of NbFP=200 and IFBW=1 kHz (corresponding to SNR of ca. 40dB) have been selected to allow fast and reliable measurements, while the effects of noise are suppressed by curve-fitting of the raw |S21| results to a Lorentz resonance curve. It has been shown that:

- post-processed results reduce the spread of material parameters (compared to raw measurements), and reveal the actual losses (otherwise underestimated due to the noise),
- material parameters extracted from the post-processed fast FieldFox measurements are in excellent agreement with the reference LabVNA measurements complying with the standards [5,6],
- measurement efficiency is improved ca.50 times, compared to measurements taken with low IFBW settings of FieldFox.

While some of our parameter choices have been based on intuitively selected data sets, the complete data will be uploaded on the MMAMA website [17], in accordance with the EC requirements for Open Innovation. This will also facilitate more rigorous data statistics by future researchers.

ACKNOWLEDGMENT

This project has received funding from the European Union's Horizon 2020 research and innovation programme (H2020-NMBP-07-2017) under grant agreement MMAMA No. 761036.

REFERENCES

[1] J. Krupka, A. P. Gregory, O. C. Rochard, R. N. Clarke, B. Riddle, and J. Baker-Jarvis, "Uncertainty of complex permittivity measurements by split-post dielectric resonator technique", *J. Eur. Ceramic Soc.*, vol. 21, pp. 2673-2676, 2001.

[2] J. Krupka and J. Mazierska, "Contactless measurements of resistivity of semiconductor wafers employing single-post and split-post dielectric-resonator techniques," *IEEE Trans. Instr. Meas.*, vol. 56, no. 5, pp. 1839-1844, Oct. 2007.

[3] K. Tanabe, Y. Kobayashi, and S. Tanaka, "Numerical analysis of eigenvalue solution of disk resonator (short papers)," *IEEE Trans.Microw. Theory Techn..*, vol. 23, no. 6, pp. 508–511, Jun 1975.

[4] T. Karpisz, B. Salski, P. Kopyt, and J. Krupka, „W-band measurements of low-loss dielectrics with Fabry-Perot Open

Resonator", *IEEE MTT-S Intl. Microwave Symp. 2019*, pp. 1503-1506, Boston, June 2019.

[5] European Standard: IEC 61189-2-721:2015. [Online]. Available: https://webstore.iec.ch/publication/22343

[6] M. Celuch, J. Rudnicki, and J.Krupka, "Data acquisition with Split - Post Dielectric Resonators", Standard Operating Procedures, Deliverable of H2020 MMAMA project. Available: https://zenodo.org/record/2673793#.Xjc47TJKh0w

[7] P. Kopyt, B. Salski, P. Zagrajek, D. Janczak, M. Sloma, M. Jakubowska, M. Olszewska-Placha, and W. Gwarek, "Electric properties of graphene-based conductive layers from DC up to Terahertz range," *IEEE Trans. THz Sci. Technol.*, vol. 6, no. 3, pp. 480-490, 2016.

[8] M. Olszewska-Placha, B. Salski, D. Janczak, P.R. Bajurko, W. Gwarek, and M. Jakubowska, "A broadband absorber with a resistive pattern made of ink with graphene nano-platelets," *IEEE Trans. Antennas Propag*., vol. 63, no. 2, pp. 565-57, Feb. 2015.

[9] K. Kielbasinski, J. Szalapak, J. Krzeminski, A. Mlozniak, E. Zwierkowska, M. Teodorczyk, O. Jeremiasz, M. Jakubowska, "Aluminium silvering of high current connectors using printing techniques and nanopowders," *Proc. of the 5th Electronics System.-integration Technology Conference (ESTC)*, Sep. 2014.

[10] O. V. Kozlov, Y.N. Luponosov, A.N. Solodukhin, B. Flament, O, Douheret, P. Viville, D. Beljonne, R. Lazzaroni, J. Cornil, S.A. Ponomarenko, and M.S. Pshenichnikov, "Simple donor-acceptor molecule with long exciton diffusion length for organic photovoltaics", *Organic Electronics*, vol. 53, pp. 185-190, Feb. 2018.

[11] T. Minari ; X. Liu ; M. Kanehara, "Printable electronic circuits based on metal nanoparticles and organic semiconductors," *IEEE Intl. Conf. on Electr. Pack. and iMAPS All Asia Conference (ICEP-IAAC)*, 2018.

[12] T. Raczynski, D. Janczak, J. Jankowska-Sliwinska, M. Dawgul, A. Paziewska-Nowak, D. Pijanowska, M. Zych, and M. Jakubowska , "Screen printed graphene electrodes for voltammetric dopamine determination", *Proc. Photonics Applications in Astronomy, Communications, Industry, and High-Energy Physics Experiments 2019*, Wilga, Nov. 2019.

[13] M.D. Tyona, "A theoretical study on spin coating technique," *Advances in Materials Research*, vol. 2, no. 4, pp.195-2018, 2013.

[14] M. Celuch, "Dielectric resonator scanning of wafer-size surfaces at finer – than – head resolution", *Microwave Characterization and Modelling at Nano and Micro-Scale of Advanced Materials to Enhance Emerging Products Manufacturing Workshop, European Microwave Week* 2019, Paris, Oct. 2019.

[15] M. Celuch, O. Douheret, P. Korpas, R. Michnowski, M. Olszewska-Placha, and J. Rudnicki, "Portable low-cost measurement setup for 2D imaging of organic semiconductors," accepted for *IEEE MTT-S Intl. Microwave Symp. 2020.*

[16] P. Korpas, W. Wojtasiak, J. Krupka, and W. Gwarek, "Inexpensive approach to dielectric measurements," *Proc. 19th Intl. Microwave and Radar Conf. MIKON*, pp. 154-157, Warsaw, May 2012.

[17] H2020 MMAMA project. [Online]. Available: https://www.mmama.eu

[18] M. Celuch, W. Gwarek, and A. Wieckowski „Enhanced-resolution material imaging with dielectric resonators: a new Implicit Space-Domain Technique ", *IEEE MTT-S International Microwave Symposium 2019*, pp. 55-58, Boston, June 2019